Development of gullies on the landscape: A model of headcut retreat resulting from plunge pool erosion

Javier H. Flores-Cervantes,[1] Erkan Istanbulluoglu,[2] and Rafael L. Bras[1]

Received 17 August 2004; revised 13 September 2005; accepted 4 November 2005; published 14 February 2006.

[1] Head advance due to plunge pool erosion is a common process in gullies incising resistant soils. A model of headcut retreat resulting from plunge pool erosion is developed and implemented in the channel-hillslope integrated landscape development (CHILD) model, an existing three-dimensional landscape evolution modeling framework. The model estimates horizontal headcut retreat as a function of discharge, height of the headcut, upstream slope, and relevant land surface and soil properties for soil erosion. We analyze the sensitivity of headcut retreat to flow discharge, upstream slope and surface roughness, and headcut height. CHILD simulations indicate that headcut retreat is most significant in zones with either gentle slopes or large headcut heights. Model parameters have contrasting effects on the retreat rates depending on the size and depth of the pool beneath the headcut and upstream flow hydraulics, making the process difficult to predict as a function of topographic thresholds and simple geomorphic transport laws.

Citation: Flores-Cervantes, J. H., E. Istanbulluoglu, and R. L. Bras (2006), Development of gullies on the landscape: A model of headcut retreat resulting from plunge pool erosion, *J. Geophys. Res.*, *111*, F01010, doi:10.1029/2004JF000226.

1. Introduction

[2] Channel head locations result from a delicate balance between the erosive forcing of climate and tectonic uplift and the resistance of the local surface to erosion and slope driven processes that tend to fill channels on the landscape [*Smith and Bretherton*, 1972; *Kirkby*, 1993, 1994; *Moglen et al.*, 1998]. This balance can be disturbed with changes or fluctuations in the forcing, land use practices, and vegetation disturbances. Sometimes channels advance rapidly to unchanneled hillsides through a combination of processes often known as gully erosion [*Higgins et al.*, 1990; *Prosser and Soufi*, 1998]. Arguably, gully erosion continues until the balance between forcing and resistance is reestablished, which may take several years, decades, or even centuries, as in the case of arroyo development in the U.S. southwest [*Bull*, 1997].

[3] Understanding the factors that control the rate of channel head advance is among the open questions in geomorphology. *Horton* [1945] proposed that an erosion threshold controls the location of channel heads, suggesting that the critical distance below the topographic divide required for sheet flow erosion is the same as that required for channel incision. *Montgomery and Dietrich* [1988, 1989, 1994], *Dietrich et al.* [1993], and *Montgomery* [1994, 1999] identified erosion by saturation overland flow and pore pressure induced landsliding responsible for maintaining gully heads in a soil-mantled, moderate-relief humid landscape. Other processes at the channel head include piping and seepage erosion [*Dunne*, 1980; *Howard and Mclane*, 1988; *Howard*, 1995], and mass wasting of sidewalls [*Dietrich and Dunne*, 1993; *Montgomery*, 1999].

[4] Through a series of flume experiments and theory, *Bennett* [1999], *Bennett et al.* [2000], *Bennett and Casalí* [2001], *Alonso et al.* [2002], *De Ploey* [1989], *Stein and Julien* [1993, 1994], *Stein et al.* [1993] and *Dey et al.* [2001], studied gully head retreat due to plunge pool erosion. Plunge pool erosion is the scouring of a hole resulting from water falling into a pool from a vertical scarp. Generally these pools develop in scarps that occur along ephemeral or perennial water courses, and the pool scouring often results in the incision of a channel as deep as the scarp's height. These scarps later become the head of a channel incising the land and are commonly referred to as headcuts. Two mechanisms of headcut retreat (also known as headcut upstream migration) resulting from plunge pool erosion have been observed: that where the headcut face translates at a constant rate (e.g., that observed by *Bennett* [1999]) and that where migration occurs due to episodic cantilever failures (e.g., that investigated by *Stein and La Tray* [2002]). The first mechanism occurs in homogeneous soils, while the second in stratified soils consisting of a top cohesive and resistant layer (such as clays) and a bottom layer of easily eroded material.

[5] The type of plunge pool erosion discussed in this paper is that occurring in homogeneous soils. This type of retreat results in the continuous migration of a headcut face and the plunge pool beneath it. As the water jet

[1]Department of Civil and Environmental Engineering, Massachusetts Institute of Technology, Cambridge, Massachusetts, USA.
[2]Department of Geosciences and Department of Biological Systems Engineering, University of Nebraska at Lincoln, Lincoln, Nebraska, USA.

0148-0227/06/2004JF000226

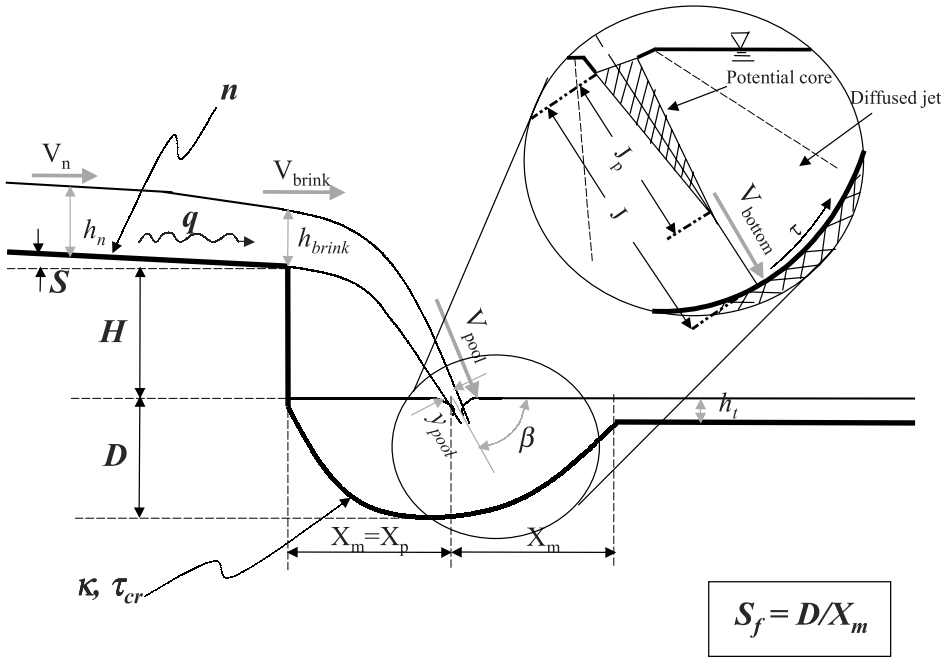

Figure 1. Scheme of the headcut-plunge-pool system.

penetrates the pool and reaches its bottom, the jet divides into two jets parallel to the bed of the pool and scour it. One of these parallel jets scours in the downstream direction, where the maximum shear stress occurs. The other parallel jet, in the upstream direction, entrains material along the face of the headcut and along the scour hole due to the vorticity of an upstream captive eddy. Recent experimental results [*Bennett et al.*, 2000; *Bennett and Casalí*, 2001] on the growth and migration of headcuts using typical upland soils suggest that headcut retreat attains a steady state, during which headcut geometry, migration rate, and sediment yield at the headcut remains constant [*Alonso et al.*, 2002]. In this paper we extent the theory described in the earlier works and implement a steady state model for headcut retreat in the channel-hillslope integrated landscape development (CHILD) model [*Tucker et al.*, 2001].

[6] Through this modeling effort we explore the topographic conditions that make headcut retreat due to plunge pool erosion likely. For gully erosion to be active and erode unchanneled surfaces, a step change in elevation (the headcut) has to be maintained on the landscape. We hypothesize that a headcut is maintained on the landscape when retreat rate is faster than water driven erosion at the brink, which tends to reduce the headcut height.

[7] The headcut retreat model is described in the following section. Section 3 explores the sensitivity of the model to different hydraulic conditions and the threshold conditions for plunge pool erosion (and thus retreat). In section 4, simulations of the model in CHILD are presented. These simulations aim to explore the combination of topographic conditions that contribute to headcut retreat development in the landscape. The results of the simulations are presented and discussed in Section 5. In addition, we discuss how the headcut retreat model compares with experimental observations. Section 6 presents the conclusions derived from this work.

2. Model Description

[8] The model calculates the retreat rate of a headcut as a function of given flow and other physical environment conditions. When implemented in a landscape evolution model, headcut retreat contributes to the shaping of the landscape along with other geomorphic erosive processes.

[9] The rate of retreat $\frac{dX}{dt}$ is modeled as a function of the rate of vertical deepening of the plunge pool $\frac{dD}{dt}$ divided by a shape factor, S_f, as

$$\frac{dX}{dt} = \frac{1}{S_f}\frac{dD}{dt}, \tag{1}$$

where X is the horizontal retreat length, t is time and D the depth of the pool. The shape factor S_f is the ratio of depth D to the pool's mid length X_m, $S_f = D/X_m$ (see Figure 1). This ratio depends on the soil type and varies between 0 and ~1. For example, *Stein and La Tray* [2002] found a D/X_m ratio of 0.56 for Ottawa sand, invariant with time of scour, scour hole size, and discharge. This formulation assumes that as the headcut retreats the shape of the pool remains constant. This implies that exactly enough material produced by the retreating head is deposited in the downstream end of the pool to keep the shape of the pool constant. In addition, this formulation does not explicitly consider any specific type of mechanism for the erosion of the scarp face. However, relating retreat to the deepening of the plunge pool arguably implies both erosion along the scarp face due to the vorticity of the upstream captive eddy and potential instabilities in the scarp face due to undermining.

[10] The rate of deepening, $\frac{dD}{dt}$, is estimated as a function of the maximum shear stress produced at the bottom of

the pool, τ, in excess of a critical value [*Stein et al.*, 1993], as

$$\frac{dD}{dt} = \kappa(\tau - \tau_{cr})^p, \ \tau > \tau_{cr}, \tag{2}$$

where κ is soil erodibility, τ_{cr} is the critical shear stress required for scouring of the soil, and p is an empirical exponent commonly 1 for cohesive soils [*Alonso et al.*, 2002; *Stein and Julien*, 1994; *Stein et al.*, 1993].

[11] The shear stress at the bottom of the pool is caused by a steady state discharge of water falling from the headcut into the plunge pool. We adopted the approach followed by *Alonso et al.* [2002], *Stein et al.* [1993], and *Stein and Julien* [1994] to calculate this shear stress, where shear stress is a function of a friction factor and the flow velocity at the bottom of the pool:

$$\tau = C_f \rho V_{bottom}^2, \tag{3}$$

where C_f is a coefficient of friction, ρ is the density of water, and V_{bottom} is the flow's maximum velocity produced by an impinging jet at the pool's bed (Figure 1). Following *Alonso et al.* [2002], a Blasius flow assumption (irrotational flow along a flat surface) can be used to obtain C_f;

$$C_f = 0.025\left(\frac{\nu}{q}\right)^{0.2}, \tag{4}$$

where q is the discharge at the brink per unit width of the headcut and ν is the kinematic viscosity of water.

[12] The velocity at the bottom of the pool (V_{bottom}) is a function of the velocity of the water jet impinging into the pool's surface, V_{pool}, and the level of turbulence-driven diffusion, if any, as the jet travels across the water body (Figure 1). Flow velocity remains constant and equal to the impinging velocity (V_{pool}) along the jet centerline, for a distance J_p, in a zone often known as the potential core [*Stein et al.*, 1993] (Figure 1). When the distance along the jet centerline between the point the jet impinges the pool and the point it impinges the bed, J, is smaller than J_p, the potential core reaches the bottom of the pool, meaning that no diffusion (of the centerline velocity) occurs as the jet travels from the top to the bottom of the pool. Thus jet velocity at the bottom of the pool (V_{bottom}) is equal to the velocity at the pool's surface (V_{pool}). This condition at the pool is hereafter referred to as a "nondiffusion state." In contrast, when J is larger than J_p, the flow velocity along the jet centerline is reduced by diffusion, and this condition is hereafter referred to as a "diffusion state." Now we can express V_{bottom} based on these conditions as

Nondiffusionstate

$$V_{bottom} = V_{pool}, J \le J_p, \tag{5}$$

Diffusionstate

$$V_{bottom} = C_d\sqrt{\frac{y_{pool}}{J}}V_{pool}, J > J_p, \tag{6}$$

where y_{pool} is the thickness of the jet as it impinges into the pool (Figure 1, $y_{pool} = \frac{q}{V_{pool}}$), and C_d is a diffusion coefficient [*Stein et al.*, 1993] that varies between 2.5 to 2.72 when the jet impinges in flat surfaces, according to *Beltaos*' [1976] and *Beltaos and Rajaratnam*'s [1973] experiments. In this work we use C_d = 2.6, the value used by *Stein and Nett* [1997].

[13] Now we need to derive expressions for both J and J_p to use in equations (5) and (6). We obtain J simply using the geometry of the pool and the angle of the jet impinging the pool relative to a horizontal plane, β, (later given by (13)) (Figure 1) as

$$J = \frac{D}{\sin\beta}. \tag{7}$$

For J_p, we equate (5) and (6) and solve for J:

$$J_p = C_d^2 y_{pool}. \tag{8}$$

[14] Equation (7) requires information about the plunge pool depth D. We suggest that pool depth can be obtained once the flow velocity at the brink, V_{brink} is known. Here, for a free-falling jet, assuming that the horizontal distance from the headcut to the pool's deepest point, X_m, is equal to the horizontal distance from the headcut to the point where the jet impinges the pool, X_p, D can be calculated with

$$D = S_f X_p = S_f V_{brink}\sqrt{\frac{2H}{g}}. \tag{9}$$

In the equation the free-falling jet assumption implies $X_p = V_{brink}\sqrt{\frac{2H}{g}}$, where V_{brink} is the flow velocity at the brink of the headcut, H is the headcut height, and g is gravitational acceleration.

[15] Finally, substituting (7) into (6) and (5) and (6) into (3), the shear stress can be rewritten

$$\tau = C_f \rho V_{pool}^2 \tag{10}$$

for the condition $J \le J_p$, a nondiffusion state, and

$$\tau = \left[\frac{C_d^2 y_{pool}\sin\beta}{D}\right] C_f \rho V_{pool}^2 \tag{11}$$

for the condition $J > J_p$, a diffusion state. In equation (11) the term in brackets represents the degree of diffusion in the pool and is always less than 1. Thus the higher the degree of diffusion the smaller the shear stress and consequently the retreat rate.

[16] For ventilated jets, meaning that the jet is surrounded by an atmospheric pressure above and below [*Stein et al.*, 1993], as often the case in the field for step-like abrupt headcuts [*Oostwoud Wijdenes and Brian*, 2001; *Nyssen et al.*, 2002; *Jungerius et al.*, 2002] (Figure 1), V_{pool} can be calculated from analysis of its component vectors as

$$V_{pool} = \frac{V_{brink}}{\cos\beta}, \tag{12}$$

where β, the angle of the jet impinging the plunge pool relative to a horizontal plane (Figure 1), is

$$\beta = \arctan\frac{\sqrt{2gH}}{V_{brink}}. \tag{13}$$

[17] Up to this point, we have expressed the tractive shear stress that drives headcut retreat, as a function of the jet

Table 1. Functional Forms of Shear Stress for Each Flow Regime and Diffusion or Nondiffusion State

Upstream Flow Regime	Diffusion	Nondiffusion
Subcritical	$\tau \propto (q^{2/3})$	$\tau \propto (q^{2/3}, H)$
Supercritical	$\tau \propto (q^{0.6}, n^{0.6}, S^{-0.3})$	$\tau \propto (q^{0.8}, n^{-1.2}, S^{0.6}, H)$

velocity at the bottom of the pool, V_{bottom} (equation (3)). Next, we write V_{bottom} in terms of velocity entering the pool, V_{pool}, which appears to be a function of the velocity at the headcut brink, V_{brink} (equation (12)). Finally shear stress τ, pool depth D, and angle of impingement β, are all expressed in terms of V_{brink}. Here, in a more detailed explanation, V_{brink} represents the accelerated flow velocity on top of the headcut as the flow approaches the free overfall, along a distance typically two to four times of the normal flow depth [*Alonso et al.*, 2002; *Hager*, 1983; *Stein and Julien*, 1993]. The velocity at the brink, V_{brink}, depends on the flow regime before the flow enters the accelerated flow region. Flow regime is calculated according to the Froude Number, $Fr = \frac{V_n}{\sqrt{gh_n}}$, where V_n is the normal flow velocity, before it enters the accelerated flow region, and h_n the normal flow depth ($h_n = q/V_n$). For subcritical flows ($Fr < 1$, i.e., deeper and slower flows) the flow changes regime as it enters the accelerated flow region, and V_{brink} is only a function of the unit discharge at the brink, q [*Rouse*, 1950]. When $Fr > 1$ (supercritical flow, that corresponds to faster and shallower flows), V_{brink} is a function of both overland flow velocity and the Froude Number [*Hager*, 1983]. These cases are written in terms of flow discharge as

$$V_{brink} = \frac{\sqrt[3]{qg}}{0.715}, \text{ for } Fr < 1. \tag{14}$$

$$V_{brink} = V_n \frac{Fr^2 + 0.4}{Fr^2} = \frac{q^{0.4} S^{0.3}}{n^{0.6}} \left(1 + \frac{0.4 n^{0.5} g^{0.5}}{q^{0.1} S^{0.45}}\right), \text{ for } Fr > 1, \tag{15}$$

[18] The flow velocity upstream of the brink (V_n) is calculated using Manning's equation as a power function of overland discharge and local slope ($V_n = n^{-0.6} q^{0.4} S^{0.3}$, where n is the Manning's roughness coefficient and S is the slope, both upstream of the headcut (Figure 1)).

[19] The model described above relates velocity at the brink V_{brink}, and hence the retreat rate, to surface slope, roughness, and flow discharge, when the flow upstream of the headcut is supercritical. In the case of subcritical flows, V_{brink}, and consequently the retreat rate, are independent of the first two parameters, and are only a function of flow discharge.

[20] In the model, retreat rate is related to the degree of diffusion of the jet centerline velocity (that depends on the flow conditions at the brink, the headcut height, and the pool's shape), such that the higher the degree of diffusion the smaller the retreat rate.

3. Model Sensitivity

[21] This part first investigates the sensitivity of headcut retreat to the input parameters headcut height (H), flow discharge (q), and surface roughness (n) and slope (S) upstream of the brink. We also discuss the effects of flow regime and jet diffusion on shear stress in the bottom of the pool.

3.1. Four Modes of Headcut Retreat

[22] Table 1 shows functional forms of the plunge pool shear stress for different flow regime and jet diffusion conditions in terms of their approximate proportionalities to H, q, n and S. Headcut retreat rates would vary depending on the overland flow regime upstream of the headcut and diffusion of the jet in the pool. It is important to explore both the sensitivity of plunge pool erosion to internal and external factors under these different flow regime and jet diffusion conditions, and the factors that cause the shift among different modes of headcut retreat (Table 1). Here we first attempt to quantify the conditions at the boundary of different shear stress formulations (Table 1).

[23] For a given set of model input parameters, Figure 2 plots the boundary between the diffusion and nondiffusion states in a discharge versus headcut height ($q - H$) space as a bold black line, as well as the lines of constant shear stress in each region. In the case when flows are relatively small over large headcuts (top left zone on the plot), the centerline velocity of the jet impinging into the plunge pool diffuses, implying a dampening of the erosive power of the impinging jet and thus a slower headcut retreat. No reduction in the centerline velocity of the jet occurs under large flows over

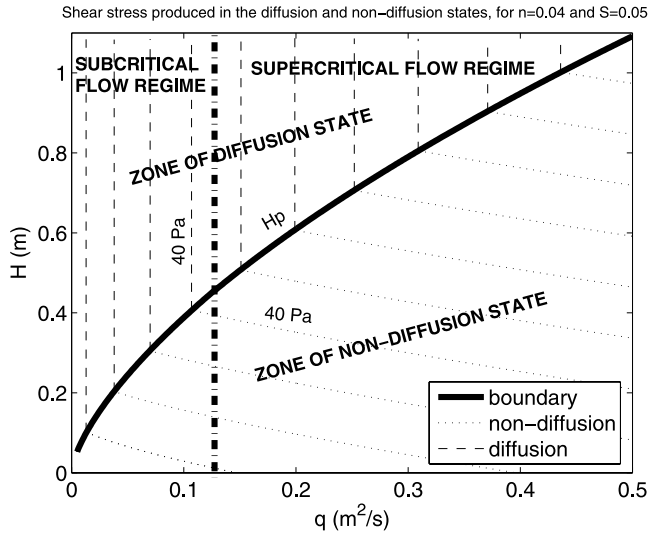

Figure 2. Shear stress at the bottom of the plunge pool as a function of q and H for $n = 0.04$, $S = 0.035$, and $S_f = 0.5$ in each of the four modes of plunge pool erosion: (a) diffusion and (b) nondiffusion states in a subcritical flow regime and (c) diffusion and (d) nondiffusion in a supercritical flow regime. The boundary between the diffusion and nondiffusion zones is represented by a thick solid line and corresponds to the values of H_p for the different discharge values. The boundary between the subcritical and supercritical flow regimes is represented by a vertical dot-dashed line that corresponds to flow conditions where $Fr = 1$. In the diffusion zone each vertical dashed line represents shear stress in intervals of 10 Pa, increasing as flow increases. In the nondiffusion zone each dotted line represents shear stress in intervals of 10 Pa, increasing in the upward direction.

relatively small headcuts, (bottom right zone on the plot). Note that the domain is also subdivided to sub and supercritical flow regions, and combined with the boundary line between diffusion and nondiffusion, this divides the domain into four regions. In plotting the shear stress we used the appropriate forms for each of the four regions (equations (19), (20), (22) and (23)) as described in the following text. This diagram is independent of n and S in a subcritical flow regime, but it is sensitive to these parameters under supercritical conditions. The plot shows how the shear stress in the diffusion and nondiffusion zone depend differently on q and H.

[24] The boundary between the two distinct zones, diffusion and nondiffusion, is the solution of the headcut height for a given discharge that makes $J = Jp$ (equations (7) and (8), Figure 1). In order to derive this equation we first obtained expressions for shear stress under diffusion and nondiffusion states in terms of the flow velocity at the headcut's brink V_{brink} and H (later, V_{brink} is decomposed into a function of q, and of q, S, and n, depending on the flow regime upstream of the brink) as follows:

Diffusion state

$$\tau = \frac{C_d^2 C_f \rho q g}{S_f V_{brink}}, \tag{16}$$

Nondiffusion state

$$\tau = C_f \rho \left(2Hg + V_{brink}^2\right). \tag{17}$$

[25] The derivation of these equations is described in Appendix A.

[26] Next, equating (16) to (17) and solving for H, results in H_p, which we define as the headcut height above of which a diffusion state occurs, and below of which a nondiffusion state occurs.

$$H_p = \frac{C_d^2 q}{2 S_f V_{brink}} - \frac{V_{brink}^2}{2g}. \tag{18}$$

[27] Equation (18) is only valid when the first term in the equation is larger than or equal to the second term. When the second term is larger, then $H_p = 0$, meaning that diffusion of the jet will occur independently of the headcut height.

[28] In the above equations, for supercritical flow upstream of the brink, V_{brink} is a function of discharge, surface roughness, and local slope at the top of the headcut, but only a function of discharge for a subcritical flow. In order to isolate the effects of these variables on shear stress in the pool under different flow regime conditions, we now define the equations presented above in terms of the components of V_{brink}.

[29] For subcritical flow, substituting (14) into (16) for the diffusing jets, and into (17) for nondiffusing flow jets, we obtain the shear stress expressions for diffusion and nondiffusion states:

Diffusion

$$\tau = \frac{0.715 C_d^2 C_f \rho g^{2/3}}{S_f} q^{2/3}, \tag{19}$$

Nondiffusion

$$\tau = C_f \rho \left(2Hg + \frac{q^{2/3} g^{2/3}}{0.715^2}\right). \tag{20}$$

Then equating (19) to (20) (alternatively substituting (14) into (18)), gives us the headcut height that defines the boundary between diffusion and nondiffusion regions as a function of discharge, for the subcritical regime.

$$H_p = \frac{1}{2g^{1/3}} \left(\frac{0.715 C_d^2}{S_f} - \frac{1}{0.715^2}\right) q^{2/3}. \tag{21}$$

[30] Similarly, for supercritical flow, we obtain the shear stress expressions by substituting the corresponding expression for V_{brink}, equation (15), written in terms of q, n and S, into equations (16) and (17), resulting in

Diffusion

$$\tau = \frac{C_d^2 C_f \rho g n^{0.6} q^{0.6} S^{-0.3}}{S_f} \left(1 + \frac{0.4 n^{0.9} g^{0.5}}{q^{0.1} S^{0.45}}\right)^{-1}, \tag{22}$$

Nondiffusion

$$\tau = C_f \rho \left(2Hg + n^{-1.2} q^{0.8} S^{0.6} \left(1 + \frac{0.4 n^{0.9} g^{0.5}}{q^{0.1} S^{0.45}}\right)^2\right). \tag{23}$$

[31] Furthermore, by equating (22) to (23) (alternatively substituting (15) into (18)) we obtain the headcut height that for a given discharge, defines the boundary between diffusion and nondiffusion regions for the supercritical regime, as plotted in Figure 2.

$$H_p = \frac{C_d^2 q^{0.6} n^{0.6}}{2 S_f S^{0.3}} \frac{1}{1 + \frac{0.4 n^{0.9} g^{0.5}}{q^{0.1} S^{0.45}}} - \frac{q^{0.8} S^{0.6}}{2 g n^{1.2}} \left(1 + \frac{0.4 n^{0.9} g^{0.5}}{q^{0.1} S^{0.45}}\right)^2. \tag{24}$$

[32] Although equations (21) and (24) seem to be different, the boundary line plotted in Figure 2 that separates the diffusion from the nondiffusion zone does not exhibit any discontinuity. If equation (21) were continued in the supercritical region for purposes of comparison, it would plot slightly higher than equation (24) (not shown in Figure 2), for the given model inputs.

[33] Figure 2 plots constant values of shear stress τ as a function of q and H in both diffusion and nondiffusion zones. In the case of jet diffusion τ is directly proportional to $q^{2/3}$ in the subcritical regime (equation (19)), and approximately to $q^{0.6}$ in the supercritical regime (equation (20)), inversely proportional to S_f, and is not related to H. Indeed, equal shear stress plots as a straight vertical line (dashed lines) in the $q - H$ space, showing that headcut retreat is independent of H. The increasing spacing between the subsequent dashed lines of constant shear stress in the diffusion zone shown in Figure 2 illustrates the nonlinear dependency between q and τ.

[34] In the nondiffusion state, τ is directly proportional to H, to $q^{2/3}$ in a subcritical flow regime (equation (20)), and approximately to $q^{0.8}$ in a supercritical regime (equation (23)) and independent of S_f. Accordingly, equal shear stress lines, which plot as oblique lines, are equidistant from each other along the H axis direction (dotted lines), illustrating the linear dependency of τ to H. These oblique lines also

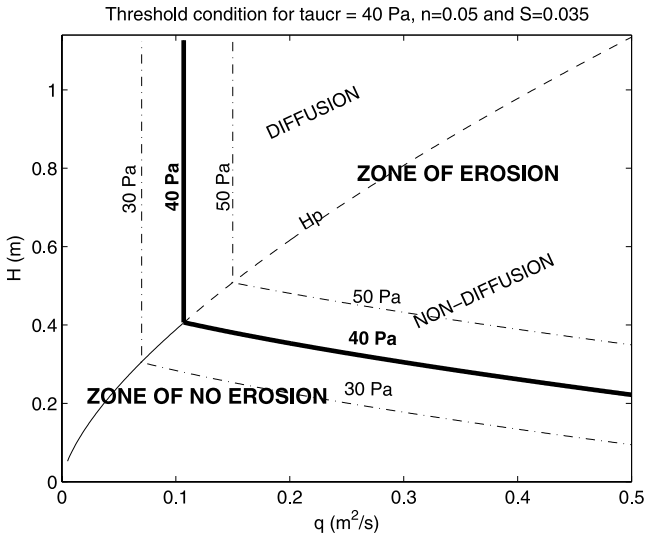

Figure 3. Threshold conditions for plunge pool erosion in terms of headcut height H and discharge q for $\tau_{cr} = 40$ *Pa*, $S = 0.035$, $n = 0.05$, and $S_f = 0.5$. The flow regime under these flow conditions is subcritical for the range of discharge shown.

show that as q increases, a smaller H is needed to maintain the same τ.

[35] Note that under a constant headcut height and discharge, the plunge pool erosion state can change from a diffusion state to a nondiffusion state or vice versa when the flow conditions upstream of the brink are supercritical. Under these supercritical conditions, changes in slope or surface roughness will alter H_p, the headcut height above which diffusion occurs and below which nondiffusion occurs (equation (24)), causing the state transitions. Under a subcritical flow regime, such transitions are not possible because H_p is a function of discharge only (equation (21)).

[36] Shear stress, τ, both in diffusion as well as nondiffusion is a function of V_{brink} (equations (16) and (17)). As V_{brink} increases, water falls further away from the headcut with a larger impinging velocity in the pool, because of the velocity's larger horizontal component. Consequently, under the steady state assumption of retreat rate, this increases the size of the plunge pool. Interestingly, an increase in V_{brink} has different consequences in τ depending on the diffusion or nondiffusion state of the jet. In a diffusion state, a larger velocity at the brink (V_{brink}) (and consequently a larger pool size and depth (D)), results in a greater diffusion of the impinging jet in the pool, causing a reduction in τ. Here jet diffusion in the pool offsets the effects of high velocity in the brink which would otherwise increase the shear stress in the pool. In contrast, in the nondiffusion state, the increase in τ due to the faster water flow is not offset by any means. Because of the above, for a constant q, in a supercritical flow regime, headcut retreat behaves differently depending on jet diffusion. In a diffusion state headcut retreat would be favored by conditions that produce relatively slow flow velocities (i.e., gentle slopes and high surface roughness upstream of the brink). In contrast, in a nondiffusion state, headcut retreat would be favored by conditions that produce high flow velocities, such as steep slopes and smooth surfaces. In a subcritical case, given that V_{brink} is only a function of q, headcut retreat is independent of slope or surface roughness.

3.2. Threshold Conditions for Plunge Pool Erosion

[37] The section above showed how shear stress in the pool depends differently on headcut height and discharge depending on the flow regime upstream of the brink and jet diffusion/nondiffusion state in the pool. Building on these findings, we now discuss threshold conditions for the trigger of plunge pool erosion on the $q - H$ domain. We attempt to derive a threshold headcut height as a function of discharge (or area surrogate to discharge) and slope, as in the threshold for channel incision concept derived by *Montgomery and Dietrich* [1989], and the threshold height for mass failure of gully walls presented by *Istanbulluoglu et al.* [2005]. For a given set of parameters, Figure 3 shows a zone of erosion and a zone of no erosion, separated by a thick solid line, representing the threshold headcut height as a function of discharge for both diffusion and nondiffusion states. In the zone of erosion the jet shear stress in the pool bottom is greater than or equal to a critical threshold value for plunge pool erosion. In the plot, the diffusion/nondiffusion boundary is represented by a dashed curve on the zone of erosion, and by a thin solid line on the zone of no erosion.

[38] The threshold for plunge pool erosion is estimated for the diffusion and nondiffusion states. In the case of nondiffusion (jet velocity is not reduced; $V_{bottom} = V_{pool}$), and for the sake of example for a subcritical flow regime, we derive an expression for threshold headcut height by solving equation (20) for H, with $\tau = \tau_{cr}$;

$$H_t = \frac{\tau_{cr}}{2g\rho C_f} - \frac{q^{2/3}}{g^{1/3}}, \tag{25}$$

(for the supercritical flow, H_t can be similarly derived from equation (23)).

[39] In the diffusion state, the threshold for plunge pool erosion is independent of H, as in this state shear stress in the pool does not depend on H (equation (19) for the subcritical flow), so it is represented by a vertical line parallel to the H axis (see Figure 3). H_p is the headcut height above of which a diffusion states occurs, and below of which a nondiffusion state occurs, and H_t is the headcut height threshold for erosion in a nondiffusion state. In order to locate this line along the q axis, the intersection between the H_p and H_t curves is used as a reference. At this intersection the shear stress at the bottom of the pool is the same for both diffusion and nondiffusion states. These vertical lines indicate that flow discharge controls the erosion of the plunge pool in the diffusion state. What Figure 3 suggests is that any combination of q and H plotting to the right of the vertical bold line in the case of diffusion state, and above the sloping bold line, in the case of nondiffusion state, would result in retreat by plunge pool erosion.

[40] From this plot the following can be concluded: in the diffusion zone, as long as height is larger than that required to maintain a diffusion state, changes in H have no effect on the shear stress, but changes in q have a large effect (see Figure 3); while in the nondiffusion zone

approximately the opposite is true, shear stress is sensitive to H and less sensitive to q than in the diffusion state (Figure 3). Thus, if nature behaves this way, to prevent gullying (to move toward the no erosion zone) one should decrease q in a diffusion situation (e.g, by building a dam upstream) and decrease H in a nondiffusion state (e.g, by bank sloping).

4. Three-Dimensional Simulations

[41] In order for a plunge pool to be effective, a step change in elevation (the headcut) has to remain on the landscape. We hypothesize that a headcut is maintained on the landscape when retreat rate is faster than water driven erosion at the brink, which tends to reduce the headcut height. Reduction in the scarp height may result in the termination of erosion in the pool. In this paper, we are interested in the topographic conditions that affect the competition process described above and in particular, in the topographic conditions that favor headcut retreat.

[42] In this section we explore the above hypothesis through numerical modeling using the CHILD model. In keeping the analysis simple, and with a focus on the posed hypothesis, we only consider soil wash and plunge pool erosion in the model, driven by storms of uniform rate and duration. A brief description of CHILD and the implementation of the headcut retreat rate model into CHILD, and of the sheetwash model used in this experiment follow.

[43] CHILD is a computational framework that simulates the evolution of a 3-D topographic surface across time in a series of discrete time steps along which a number of geomorphic processes interact and modify the topographic surface [*Tucker et al.*, 2001]. In CHILD, changes in elevation are expressed mathematically as

$$\frac{\partial z}{\partial t} = U(x, y, t) - \nabla q,$$

where $U(x, y, t)$ represents the base level change or tectonic uplift and can be variable in space and time, and ∇q is the sediment flux divergence, which is a function of different geomorphic sediment transport laws [*Dietrich et al.*, 2003]. These include fluvial erosion and deposition, soil creep and landsliding. Topography is represented by a triangulated irregular network (TIN) in which each node in the triangulation is associated with a Voronoi polygon (Voronoi cell). Voronoi polygons define the surface area associated with each node as well as the length of the interface between each pair of adjacent nodes.

[44] Headcut retreat resulting from plunge pool erosion is simulated in three steps in CHILD. First, by identifying, at each time step, the step changes in the topography (i.e., headcuts). Second by estimating headcut retreat. Third by modifying the elevation of the mesh elements.

[45] If the estimated retreat is small and does not exceed the length of a Voronoi cell, it is recorded in memory and added to previous retreat in that Voronoi cell. When this recorded retreat exceeds the cell's length, its elevation is reduced to represent erosion due to headcut retreat. The new elevation sets the slope of the bed of the incised channel equal to the slope of the bed immediately downstream. Our formulation implicitly assumes that a fraction of the eroded material fills the space left by the translating pool and the rest is transported downstream. In these experiments we assume that all that material transported downstream leaves the domain without deposition.

[46] Consistent with the assumption for headcut retreat, wash erosion is also assumed to be detachment limited. In our simulations,

$$\frac{dz}{dt} = \kappa\left(\rho g n^{0.6} q^{0.6} S^{0.7} - \tau_{cr}\right)^p \tag{26}$$

where κ is erodibility, ρ is the water density, g is gravitational acceleration, n is Manning's roughness coefficient, q discharge per unit width, S bed slope, τ_{cr} the critical shear stress, and p is an experimental coefficient. Here the first term in parenthesis represents overland flow shear stress. Note that the values of κ, τ_{cr} and p for wash erosion and for plunge pool erosion may be different. In these simulations, the width of the flow is assumed to be equal to the Voronoi cell width.

[47] The experiment simulated the evolution of a square land surface of 50 m by 50 m represented by a TIN mesh of 0.5 m node spacing under five different initial conditions. One side of the square is set as an open boundary, where any flux of water is assumed to be transported away. The initial surface dips toward the open boundary with an initial gradient of 3% (9% for one of the simulations) and is seeded with small random perturbations in elevation of each node. A 2 m high (0.5 m for one of the simulations) scarp runs along the open boundary. Such scarps in the field may result from channel incisions, instantaneous base level drop, or tectonic uplift. Retreating headcuts often develop along these scarps [*Bennett*, 1999].

[48] The model is iterated for one thousand storms of 30 mm/hr rate, and 1 *hr* duration. Losses due to infiltration and evapotranspiration are ignored. Discharge is calculated by routing the rainfall down the steepest descent. Uniform soil parameters of $\tau_{cr} = 1.75\ Pa$ and $\kappa = 8 \times 10^{-8}\ \frac{m}{Pas}$ are used in the simulations. These values are within the range of values of τ_{cr} and κ estimated for soils in the field [*Hanson and Simon*, 2001; *Laflen et al.*, 1991; *Nearing et al.*, 1999]. We approximated C_f by a constant value in the simulations because (1) the Blasius flow assumption is an approximation to the complex flow in the pool and thus the exact value of C_f is not known and (2) for a range of flows produced in the simulations, C_f estimated with equation (4) is of the same order of magnitude, between 0.004 and 0.01. We assumed $C_f = 0.009$. We also assumed that the soil is cohesive enough to support the scarps [*Istanbulluoglu et al.*, 2005]. The different initial conditions and parameters used in the simulations are summarized in Table 2. Figure 4 shows snapshots of a simulated surface, where gullies commence along the scarp and continue retreating into the unchanneled areas following flow avenues developed by upland wash erosion.

5. Results and Discussion

5.1. CHILD Simulations

[49] Landscape profiles extracted using an algorithm that identifies the longest flow path draining to a given outlet point, in different time slices of five CHILD simulations, are presented in Figure 5. The profiles illustrate the interaction

Table 2. Parameter Values Used in the Simulations

Figure	Initial S	n	Initial H, m	Runoff, mm/hr	S_f	C_f	κ, m/Pa s	τ_{cr}, Pa	p
5a	0.03	0.05	2	30	0.2	0.009	8×10^{-8}	1.75	1
5c	0.03	0.05	0.5	30	0.2	0.009	8×10^{-8}	1.75	1
5b	0.03	0.05	2	30	0.2	0.009	8×10^{-8}	1.75	1
5d	0.09	0.05	2	30	0.2	0.009	8×10^{-8}	1.75	1
5e	<0.03	0.05	2	30	0.2	0.009	8×10^{-8}	1.75	1

between the sheetwash and headcut retreat in the land surface.

[50] First we compare channel profiles developed by a combination of plunge pool headcut retreat and fluvial erosion (Figure 5a) with those eroded solely by fluvial process (Figure 5b). In the absence of headcut retreat (Figure 5b), scarp height in the initial profile is lowered until it disappears and the profile becomes a continuous line without any step change, and erodes through purely fluvial processes. In Figure 5a, although the headcut is lowered as in Figure 5b, it is not eliminated from the landscape. Headcut persistence is favored by retreat because as the headcut moves farther upstream, the drainage area contributing water discharge to the headcut decreases and so does the fluvial processes strength.

[51] The initial headcut height has an important impact on the type of processes that incise the land. Compare the simulations in Figures 5a and 5c. In Figure 5c the initial scarp height is 4 times smaller than in the former (every thing else is equal). While the headcut is rapidly lowered and erased by wash erosion in Figure 5c, the headcut and active retreat driven by plunge pool erosion continue in Figure 5a.

[52] In Figure 5d we used the same initial scarp height as in Figure 5a but with a higher initial slope, 9% instead of the original 3 percent. This increase in the initial slope results in higher rates of fluvial erosion on the headcut, resulting in a quick lowering of the headcut height. As a consequence, the headcut is rapidly erased from the topography.

[53] In Figures 5a and 5d the flow is subcritical and so retreat is independent of slope upstream of the brink. However, if it were in a supercritical regime (resulting, for example, from a larger discharge), retreat would be a function of slope, and this could have implications in the rate of headcut lowering discussed above. For instance, in a diffusion state shear stress at the bottom of the pool would decrease with slope (equation (22)), making the retreat rate slower. A slower retreat rate implies a faster lowering of the headcut due to wash erosion. Thus, in a supercritical flow regime, in a diffusion state, a steep slope upstream of the brink would further enhance a headcut's lowering rate, and consequently its elimination from the landscape.

[54] In the above examples we have assumed initially uneroded domains subject to the instantaneous creation of a scarp. Now we investigate how headcut retreat would behave in regions eroded before the instantaneous formation of the scarp. We use a declining topography (i.e., topography undergoing runoff erosion in absence of uplift), as an initial condition, where in a large portion of the domain the bed gradient of fluvially eroded channels has adjusted to critical slopes such that the overland flow erosive force is balanced with the surface resistance. The thick solid line in Figure 5e shows a channel profile extracted from the simulation domain for the above scenario, reported in Figure 6. This channel profile has an erosion wave connecting the uplands to the lowlands. The lowlands do not respond to wash erosion because they are already in equilibrium. In this scenario, headcuts are maintained in the landscape and their retreat results in significant land incision and erosion. From the five simulations presented in this section, this is the most favorable for gullying.

[55] The scenario described above resembles the Colorado Plateau, where high uplift rates created a plateau where fluvial erosion processes are not strong due to its nearly flat

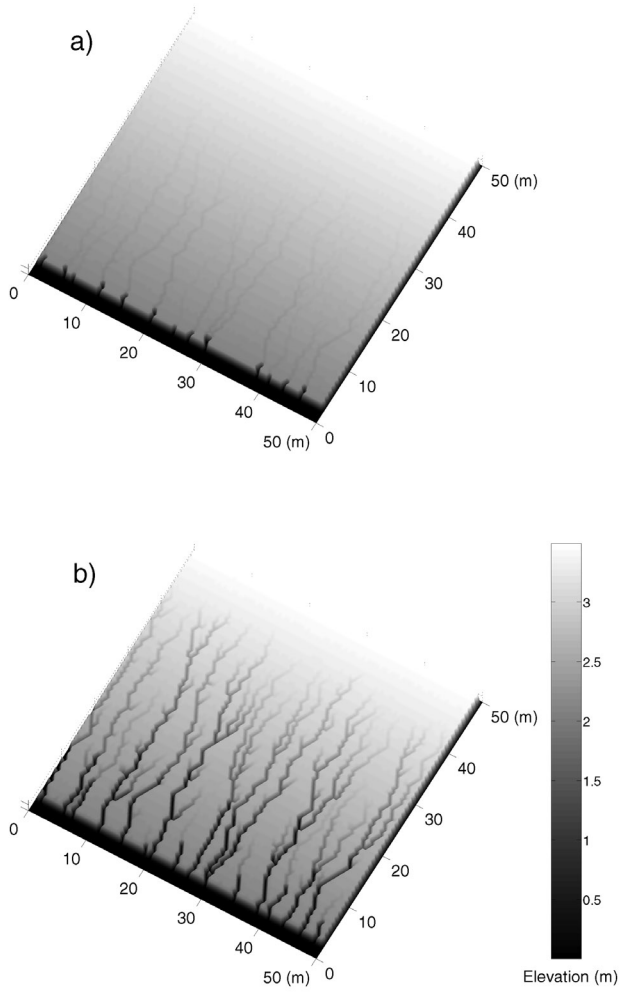

Figure 4. Elevation field of the CHILD simulation corresponding to Figure 5a after (a) one hundred and (b) one thousand 1 hr duration simulated storms.

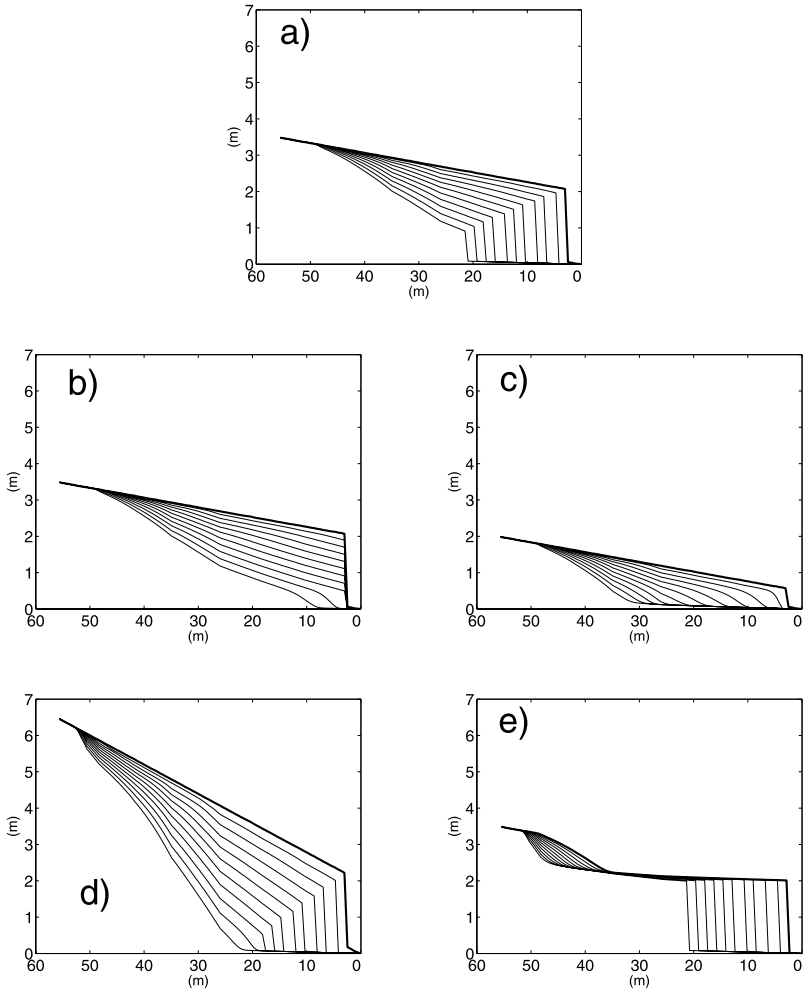

Figure 5. Profiles extracted from five CHILD simulations (see Table 2): (a) case of intermediate slope and headcut height to which the rest of the simulations presented here are compared, (b) case with no headcut retreat, (c) case with a low initial headcut, (d) case with a steep sloped surface, and (e) case of headcut retreat in a declining topography (see text) where channel profiles upstream of the headcut are nearly flat. Each line represents the channel profile in 100 hour time slices. The thick solid line indicates the initial condition. The vertical and horizontal scales are elevation above and distance from the outlet, respectively, in meters.

initial condition, and deep channels and canyons have developed. Canyons such as those studied by *Laity and Malin* [1985] arguably extend by plunge pool erosion or sapping at their heads, or a combination of both.

[56] We recognize that factors other than topographic conditions can contribute to the lowering rate of the headcut. For example, a resistant layer on top of headcuts, which can be the consequence of a well developed vegetation cover, often reduce this lowering [*Gardner*, 1983; *Schumm*, 1999; *Prosser and Slade*, 1994; *Stein and La Tray*, 2002].

[57] Changes in flow discharge do have a large impact on the shear stress produced at the bottom of a plunge pool, and in the interaction between wash processes and headcut retreat. Figure 7 shows the shear stress produced by overland flow on top of the headcut and that produced at the bottom of the plunge pool for the initial conditions of Figure 5a. Figure 7 illustrates how the plunge pool shear stress increases much more rapidly with flow discharge than the overland flow shear stress, showing the relatively greater sensitivity of plunge pool shear stress to discharge than overland flow shear stress, for subcritical conditions and a diffusion state.

[58] We recognize that the model's assumption of constant headcut width is a limitation because retreat is sensitive to the width of the headcut. For a given total water discharge, a narrower headcut will result in a larger flow per unit width and in more intense plunge pool erosion. The width in our experiments is just 0.5 m, quite reasonable for a developing gully. A constant width facilitated implementation and computation in CHILD. In the future this limitation can be eliminated.

[59] Conclusions similar to the ones made with the 3-D simulations in CHILD were reached with simpler 1-D simulations. However, the benefit of using the 3-D model, as seen in Figure 6, is the reproduction of flow aggregation that lead to spatially variable rates of water erosion and retreat due to plunge pool erosion, forming a dendritic flow network. The 3-D approach will also be more realistic in a depositional environment.

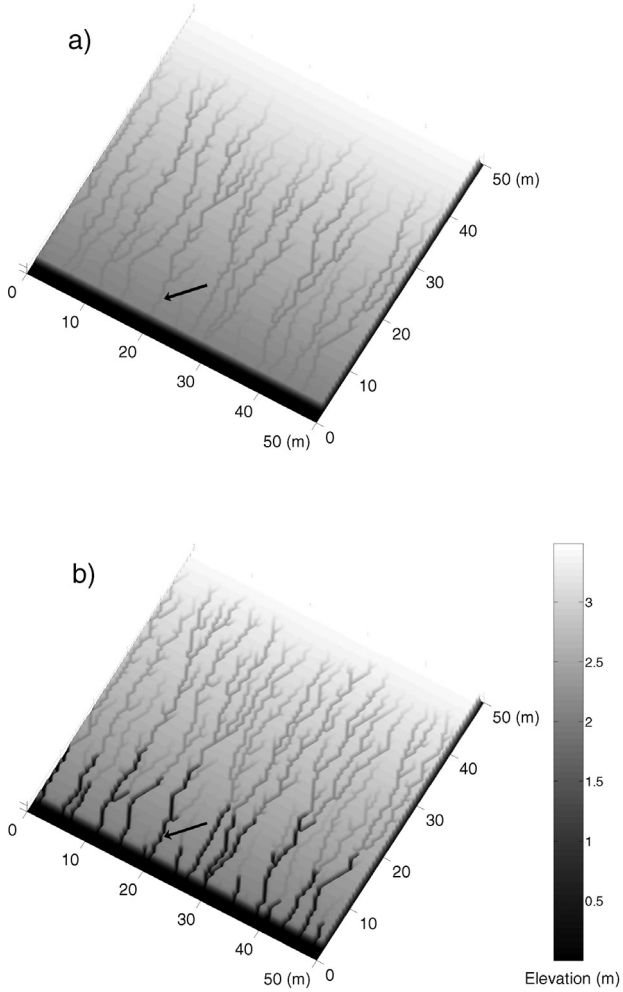

Figure 6. Elevation fields of the (a) initial and (b) final surface representations of the CHILD simulations corresponding to Figure 5e where topographic change is predominantly due to headcut retreat. This simulation corresponds to a declining topography as an initial condition, in which, in a large portion of the domain, the slopes of fluvially incised channels have adjusted to critical slopes such that the erosive force is balanced with the surface resistance. The arrow points to the outlet of the profile shown in Figure 5e.

[60] The combination of processes we investigate have been explored before at the University of Colorado, Fort Collins, by *Begin et al.* [1980a, 1980b] by means of physical experiments. *Begin et al.* [1980a, 1980b] conducted their experiments in a 20 m long flume and a 15 m by 7 m container. The initial conditions of their experiments consisted of a gently sloping surface (1%) that dipped toward a scarp where a lowering in base level was simulated. During the initial stages of their experiments, sheetwash formed rills on the flat surfaces, and gullying due to headcut retreat developed along these rills starting at the scarp, in a fashion similar to that of Figure 4. However, during the later stages of the experiments, gully widening due to the collapse of the gully banks occurred. The consequent excess of bank material in the channel hampered headcut retreat until retreat stopped.

[61] A bank failure mechanism has been implemented and explored in CHILD [*Istanbulluoglu et al.*, 2005]; therefore exploring the effect of the three processes observed in Begin's experiments, wash erosion, headcut retreat, and bank failures, where the flow's sediment transport capacity is taken into account, is the next logical step in this line of investigation of the processes.

5.2. Flume Experiments

[62] *Bennett* [1999] and *Bennett and Casalí* [2001] conducted a series of flume experiments to examine the effects of bed slope, and the effect of initial headcut height, on the growth, development and upstream migration of headcuts. In each of these series they systematically varied the variable of interest (bed slope or initial headcut height) while maintaining the rest of the experimental conditions constant. These flume experiments involved headcuts that were relatively small, of the order of few millimeters to a few centimeters high. Normally channels of this size would not be classified as gullies [*Brice*, 1966], however they are formed by the same mechanisms observed in larger gullies, and could be referred to as small, rill-like gullies [*Higgins et al.*, 1990].

[63] In some of Bennett and colleagues' flume experiments, the flow jet was nonventilated, meaning that the jet was submerged in the flow. Since the model described in this paper is for ventilated jets we eliminated the data collected under nonventilated conditions in our comparison. The comparison of model predictions of retreat rates against the observed rates is hampered by the lack of information for flow roughness, soil erodibility and critical shear stress.

[64] Major input parameters in the model reported by Bennett and coworkers are flow discharge (q), initial headcut height (H), and bed slope (S). We also use reported upstream flow depth and velocity to estimate Manning's roughness (n), and reported maximum scour depth, length to the maximum scour depth from the scarp, and scarp

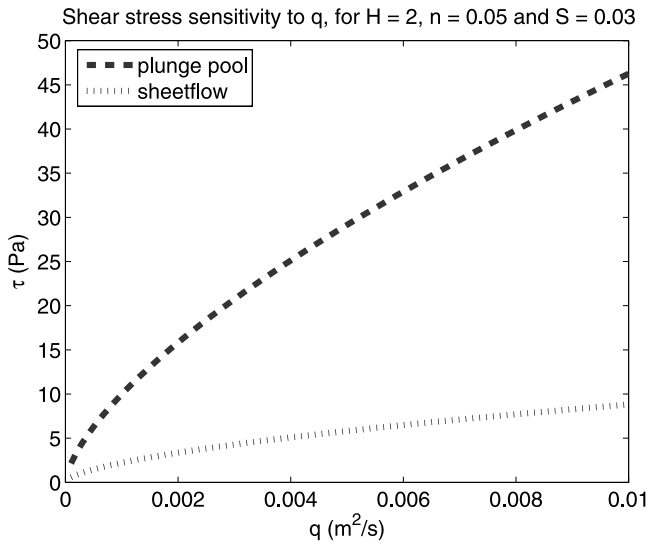

Figure 7. Plunge pool and sheet flow shear stresses, as functions of discharge, for $H = 2$ m, $n = 0.05$, and $S = 0.035$. These conditions correspond to a diffusion state and a subcritical flow regime.

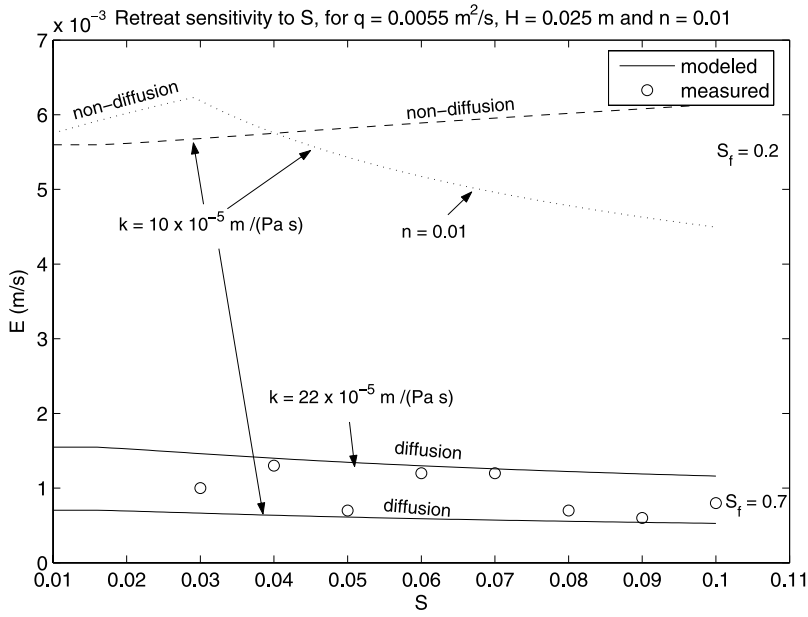

Figure 8. Measured and modeled retreat rates for different values of bed slope. The measured values are from experiments carried out in a flume by *Bennett* [1999]. For the conditions reported in Bennett's experiment the model's retreat rate slightly decreases as the bed slope increases. The experimental observations suggest little variability in the retreat rate which seems to be in agreement with the model. The model predicts a diffusion state, with a supercritical flow regime upstream of the brink, consistent with the flow characteristics reported by *Bennett* [1999]. Examples of retreat rates predicted by the model under circumstances different from the flume experiments are also explored (smaller S_f and n, see text).

height, to calculate the shape factor (S_f). While these estimated values show some variation from one run to another, we used their averages as representative of central tendency conditions.

[65] Figure 8 plots headcut retreat rate versus bed slope, reported by *Bennett* [1999] for one of his experiments. In this experiment flow regime upstream of the headcut is supercritical, with some degree of jet centerline velocity diffusion in the pool. Shear stress under these flow conditions can be calculated using equation (22). The friction coefficient C_f is obtained from equation (4). Solid lines graph the calculated retreat rates with erodibility values fitted to cover the range of variation in the data. The soil used in these experiments is highly erodible; thus we assume $\tau_{cr} = 0$ *Pa*. In Figure 8 a higher, nonzero, critical shear stress would shift the retreat rate down. For a diffusion state, the model predicts little change in retreat rate with slope, as observed in the experiments.

[66] On the slope retreat rate space the flow regime and the degree of jet diffusion inside the pool result in marked differences. With a 65% reduction in shape factor, retreat occurs in a nondiffusion state, plotting positively with bed slope (dashed line). Reducing the Manning's roughness coefficient to half the original (making the surface smoother), results in a nondiffusion state for slopes smaller than ~3%, and is positively related to the bed slope. The rate reaches a maximum at ~3%, and then decreases with slope as the process switches to a diffusion state, for slopes higher than ~3%. Note that here 3% is only a model result for a given set of parameters. In a subcritical regime, where retreat is insensitive to changes in slope, retreat would plot as a straight horizontal line (not shown).

[67] The experimental data does not show any trend in retreat rate as a function of headcut height (Figure 9). The model also predicts no change in the retreat rate with headcut height, using the same range of erodibility as in Figure 8. In the model this lack of sensitivity of retreat rate is due to a reduction of the jet's velocity at the pool due to diffusion (equation (6)). As derived in equation (22), shear stress in the pool is independent of headcut height when jet velocity is reduced by diffusion in the pool. Note that in Figure 9 the threshold headcut height between a diffusion and a nondiffusion state, H_p, calculated using the data of *Bennett and Casalí* [2001] (equation (24)), is 0.032 m. Below this threshold the theory predicts retreat to be a function of H, as shown in Figure 9. Figure 9 also shows that when the model is forced to a nondiffusion state for the range of headcut heights of the experimental data, by reducing the shape factor but maintaining the rest of the model input values constant, retreat plots directly proportional to headcut height for the whole range of H analyzed in Figure 9.

[68] It is important to note that Bennett reports an increase in headcut heights, from the initial heights, during some of his experiments reported in Figure 8. This is not a problem for the model's test since in the diffusion state horizontal retreat rate is independent of the headcut height.

6. Conclusions

[69] We have presented a headcut retreat model where retreat is due to plunge pool erosion. This model is based on earlier work of *Bennett* [1999], *Bennett et al.* [2000],

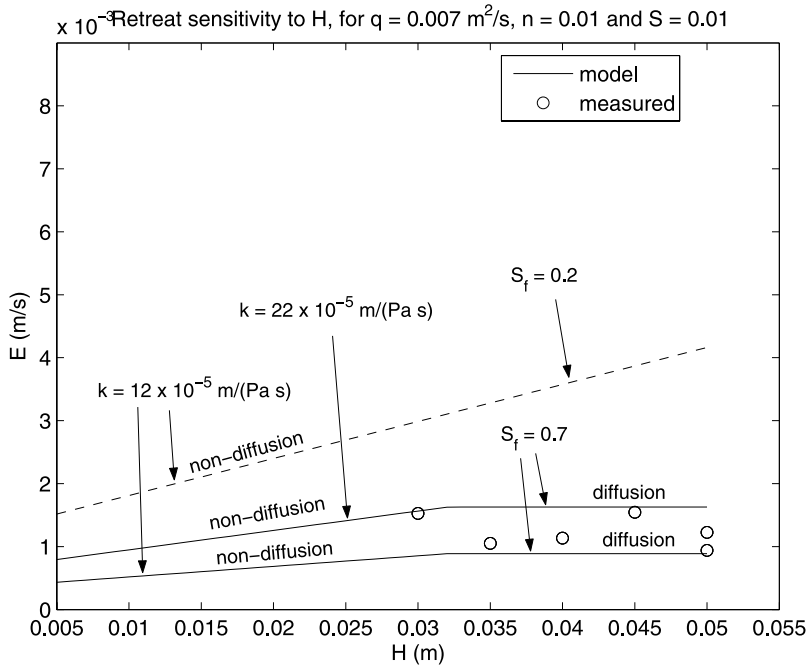

Figure 9. Measured and modeled retreat rates for different values of headcut height. The measured values are from experiments carried out in a flume by *Bennett and Casalí* [2001]. The model predictions are in agreement with the lack of change in the retreat rate observed as H increases. The model predicts a diffusion state, with a supercritical flow regime upstream of the brink, consistent with the flow characteristics reported by *Bennett and Casalí* [2001]. Figure 9 also shows how the predicted retreat rates vary under different circumstances for smaller values of headcut height and different values of S_f. In these different circumstances the model predicts a nondiffusion state.

Bennett and Casalí [2001], and *Stein and Julien* [1993, 1994] and considers the effect of discharge, headcut height, surface roughness and slope upstream of the headcut, and relevant soil parameters. We have implemented this model in a 3-D landscape evolution modeling framework, CHILD. In the model we consider the effects of diffusion of the jet inside the plunge pool. The sensitivity of retreat to variables considered, and the differences between the diffusion and nondiffusion states, are discussed. In a diffusion state the erosional potential of a jet impinging into a plunge pool is reduced, and in this state retreat is independent of headcut height but is sensitive to discharge. In a nondiffusion state retreat is sensitive to headcut height and slightly sensitive to discharge. This finding may have implications for land management practices. For example, to prevent gullying the most effective approach would be to reduce discharge in a diffusion state (e.g, by building a dam upstream of the headcut), but in a nondiffusion state, one should reduce headcut height (e.g, by bank sloping). The model predictions of retreat rates were compared with flume experiments observations. The data reported by Bennett does not show any dependence between retreat rate and both bed slope and headcut height for the diffusion state. Consistently, the model also predicts almost no dependence between retreat rate and these geomorphic variables when jet velocity is diffused in the pool. However additional data from real-world gully knickpoints would be necessary to reach more solid conclusions.

[70] For gully erosion to be active and erode unchanneled surfaces, a step change in elevation (the headcut) should remain on the landscape. We hypothesized that a headcut is maintained on the landscape when retreat rate is faster than water driven erosion at the brink, which tends to reduce the headcut height. We carried out five simulation experiments to explore this hypothesis in CHILD. From the simulations, we concluded that headcut retreat will occur and dominate over wash processes at points along scarps where overland flow concentrates and the slopes upstream of the headcut are gentle, and where the initial scarp is high.

[71] From the sensitivity analysis we concluded that a faster flow at the headcut brink, resulting from variations in bed slope or bed roughness (such velocity increase is only possible when the flow regime upstream of the brink is supercritical), decreases the headcut retreat in a diffusion state. This suggests that headcut retreat might be of secondary importance in environments where overland flow velocity is usually high.

[72] The distinction between diffusion and nondiffusion states of this model is highlighted because the model's behavior in a diffusive state provides a reasonable explanation for the small variation in retreat as slope increases, and the absence of a relationship between the retreat rate and the initial headcut height, observed in flume experiments.

[73] Factors that also have a significant impact in headcut retreat development not considered in this work are spatial differences in the critical shear stress above and below the headcut (a resistant bed upstream of a headcut), sediment transport capacity of the flow (here assumed infinite), and the variability of the headcut width (here assumed constant and defined by node spacing). The model uses a shape

factor S_f to describe the shape of the pool and is very sensitive to it. This factor may be obtained empirically, but not theoretically. Further work in this regard would improve the applicability of the model.

Appendix A

[74] Derivation of the shear stress in the plunge pool as a function of velocity at the brink (V_{brink}), discharge (q) and headcut height (H).

[75] For the diffusion state V_{bottom} is given by (6), squaring it we may write

$$V_{bottom}^2 = C_d^2 \frac{y_{pool}}{J} V_{pool}^2. \tag{A1}$$

If we substitute y_{pool} by q/V_{pool}, (A1) becomes

$$V_{bottom}^2 = \frac{C_d^2 q}{J} V_{pool}. \tag{A2}$$

Here J is obtained by substituting (9) into (7),

$$J = \frac{S_f V_{brink}}{\sin\beta} \sqrt{\frac{2H}{g}}. \tag{A3}$$

Next, we write $V_{pool} = \frac{\sqrt{2Hg}}{\sin\beta}$ from analysis of its component vectors of V_{pool}, and substituting this expression and (A3) into (A2), we may rewrite (A2) as

$$V_{bottom}^2 = \frac{C_d^2 q g}{S_f V_{brink}}. \tag{A4}$$

Finally, substituting (A4) into (3) gives equation (16) in the paper.

[76] Recalling that for the nondiffusion case $V_{bottom} = V_{pool}$, we write $V_{pool}^2 = V_{brink}^2 + 2gH$, from analysis of the component vectors of V_{pool}, and substituting this expression in (3), we obtain (17).

[77] **Acknowledgment.** This research was supported by the U. S. Army Research Office (agreement DAAD 19-01-1-0513) and the Consiglio Nazionale della Ricerche of Italy under a collaborative agreement with MIT.

References

Alonso, C. V., S. J. Bennett, and O. R. Stein (2002), Predicting head cut erosion and migration in concentrated flows typical of upland areas, *Water Resour. Res.*, *38*(12), 1303, doi:10.1029/2001WR001173.

Begin, Z. B., D. F. Meyer, and S. A. Schumm (1980a), Knickpoint migration due to baselevel lowering, *J. Waterw. Port Coastal Ocean Div. Am. Soc. Civ. Eng.*, *106*, 369–388.

Begin, Z. B., D. F. Meyer, and S. A. Schumm (1980b), Sediment production of alluvial channels in response to base level lowering, *Trans. ASAE*, *23*, 1183–1188.

Beltaos, S. (1976), Oblique impingement of plane turbulent jets, *J. Hydraul. Div. Am. Soc. Civ. Eng.*, *102*(9), 1177–1192.

Beltaos, S., and N. Rajaratnam (1973), Plane turbulent impinging jets, *J. Hydraul. Res.*, *11*(1), 29–59.

Bennett, S. J. (1999), Effect of slope on the growth and migration of headcuts in rills, *Geomorphology*, *30*, 273–290.

Bennett, S. J., and J. Casalí (2001), Effect of initial step height on headcut development in upland concentrated flows, *Water Resour. Res.*, *37*(5), 1475–1484.

Bennett, S. J., C. V. Alonso, S. N. Prasad, and M. J. M. Römkens (2000), Experiments on headcut growth and migration in concentrated flows typical of upland areas, *Water Resour. Res.*, *36*(7), 1911–1922.

Brice, J. C. (1966), Erosion and depositon in the loess-mantled Great Plains, Medicine Creek drainage basin, Nebraska, *U.S. Geol. Surv. Prof. Pap.*, *352-H*, 255–339.

Bull, W. B. (1997), Discontinuous ephemeral streams, *Geomorphology*, *19*, 1109–1124.

De Ploey, J. (1989), A model for headcut retreat in rills and gullies, in *Arid and Semi-arid Environments Geomorphological and Pedological Aspects*, edited by A. Yair and S. Berkowicz, *Catena Suppl.*, *14* 81–86.

Dey, A. K., T. Tsujimoto, and T. Kitamura (2001), Growth and migration of headcut in heterogenous soil stratum, *Annu. J. Hydraul. Eng.*, *45*, 823–828.

Dietrich, W. E., and T. Dunne (1993), The channel head, in *Channel Network Hydrology*, edited by K. Beven and M. J. Kirkby, pp. 175–219, John Wiley, Hoboken, N. J.

Dietrich, W., D. J. Wilson, D. R. Montgomery, and J. McKean (1993), Analysis of erosion thresholds, channel networks, and landscape morphology using a digital terrain model, *J. Geol.*, *101*, 259–278.

Dietrich, W. E., D. G. Bellugy, L. S. Sklar, J. D. Stock, A. M. Heimsath, and J. J. Roering (2003), Geomorphic transport laws for predicting landscape form and dynamics, in *Prediction in Geomorphology*, *Geophys. Monogr. Ser.*, vol. 135, edited by P. R. Wilcock and R. M. Iverson, pp. 103–132, AGU, Washington, D. C.

Dunne, T. (1980), Formation and control of channel networks, *Prog. Phys. Geogr.*, *4*, 211–239.

Gardner, T. W. (1983), Experimental study of knickpoint and longitudinal profile evolution in cohesive, homogeneous material, *Geol. Soc. Am. Bull.*, *94*, 664–672.

Hager, W. H. (1983), Hydraulics of plane free overfall, *J. Hydraul. Eng.*, *109*(12), 1683–1697.

Hanson, G. J., and A. Simon (2001), Erodibility of cohesive streambeds in the loess area of the midwestern USA, *Hydrol. Processes*, *15*, 23–38.

Higgins, C. G., B. R. Hill, and A. K. Lehere (1990), Gully development, *Spec. Pap. Geol. Soc. Am.*, *252*, 139–155.

Horton, R. E. (1945), Erosional development of streams and their drainage basins: Hydrophysical approach to quantitative morphology, *Geol. Soc. Am. Bull.*, *56*, 275–370.

Howard, A. D. (1995), Simulation modeling and statistical classification of escarpment planforms, *Geomorphology*, *12*, 187–214.

Howard, A. D., and C. F. Mclane (1988), Erosion of cohesionless sediment by ground water sapping, *Water Resour. Res.*, *24*, 1659–1674.

Istanbulluoglu, E., R. L. Bras, H. Flores-Cervantes, and G. E. Tucker (2005), Implications of bank failures and fluvial erosion for gully development: Field observations and modeling, *J. Geophys. Res.*, *110*, F01014, doi:10.1029/2004JF000145.

Jungerius, P. D., J. Matundra, and J. A. M. Van de Ancker (2002), Road construction and gully erosion in West Pokot, Kenya, *Earth Surf. Processes Landforms*, *27*, 1237–1247.

Kirkby, M. J. (1993), Long term interactions between networks and hillslopes, in *Channel Network Hydrology*, edited by K. Beven and M. J. Kirkby, pp. 255–293, John Wiley, Hoboken, N. J.

Kirkby, M. J. (1994), Thresholds and instability in stream head hollows: A model of magnitude and frequency for wash processes, in *Process Models and Theoretical Geomorphology*, pp. 295–314, John Wiley, Hoboken, N. J.

Laflen, J. M., W. J. Elliot, R. Simanton, S. Holzhey, and K. D. Kohl (1991), Wepp soil erodibility experiments for rangeland and cropland soils, *J. Soil Water Conserv.*, *46*(1), 39–44.

Laity, J. E., and M. C. Malin (1985), Sapping processes and the development of theater-headed valley networks on the Colorado Plateau, *Geol. Soc. Am. Bull.*, *96*, 203–217.

Moglen, G. E., E. A. B. Elthair, and R. L. Bras (1998), On the sensitivity of drainage density to climate change, *Water Resour. Res.*, *34*, 855–862.

Montgomery, D. R. (1994), Road surface drainage, channel initiation, and slope instability, *Water Resour. Res.*, *30*(6), 1925–1932.

Montgomery, D. R. (1999), Erosional processes at an abrupt channel head: Implications for channel entrenchment and discontinuous gully formation, in *Incised River Channels*, edited by S. E. Darby and A. Simon, pp. 247–276, John Wiley, Hoboken, N. J.

Montgomery, D. R., and W. E. Dietrich (1988), Where do channels begin?, *Nature*, *336*(17), 232–234.

Montgomery, D. R., and W. Dietrich (1989), Source areas, drainage density, and channel initiation, *Water Resour. Res.*, *25*, 1907–1918.

Montgomery, D. R., and W. Dietrich (1994), A physically based model for the topographic control on shallow landsliding, *Water Resour. Res.*, *30*, 1153–1171.

Nearing, M. A., J. R. Simanton, L. D. Norton, S. J. Bulygin, and J. Stone (1999), Soil erosion by surface water flow on a stony, semiarid hillslope, *Earth Surf. Processes Landforms*, *24*, 677–686.

Nyssen, J., J. Poesen, J. Moeyersons, M. Veyret-Picot, J. Deckers, M. Haile, and G. Govers (2002), Impact of road building on gully erosion risk: A

case study from the northern Ethiopian highlands, *Earth Surf. Processes Landforms*, *27*, 1267–1283.

Oostwoud Wijdenes, D. J., and R. Brian (2001), Gully-head erosion processes on a semi-arid valley floor in Kenya: A case study into temporal variation and sediment budgeting, *Earth Surf. Processes Landforms*, *26*, 911–933.

Prosser, I. P., and C. J. Slade (1994), Gully formation and the role of valley-floor vegetation, southeastern Australia, *Geology*, *22*, 1127–1130.

Prosser, I. P., and M. Soufi (1998), Controls on gully formation following forest clearing in a humid temperate environment, *Water Resour. Res.*, *34*, 3661–3671.

Rouse, H. (1950), *Engineering Hydraulics*, John Wiley, Hoboken, N. J.

Schumm, S. A. (1999), Causes and controls of channel incision, in *Incised River Channels*, edited by S. E. Darby and A. Simon, pp. 19–33, John Wiley, Hoboken, N. J.

Smith, T. R., and F. P. Bretherton (1972), Stability and the conservation of mass in drainage basin evolution, *Water Resour. Res.*, *8*(6), 1506–1529.

Stein, O. R., and P. Y. Julien (1993), Criterion delineating the mode of headcut migration, *J. Hydraul. Eng.*, *119*(1), 37–50.

Stein, O. R., and P. Y. Julien (1994), Sediment concentration below free overfall, *J. Hydraul. Eng.*, *120*(9), 1043–1059.

Stein, O. R., and D. A. La Tray (2002), Experiments and modeling of head cut migration in stratified soils, *Water Resour. Res.*, *38*(12), 1284, doi:10.1029/2001WR001166.

Stein, O. R., and D. D. Nett (1997), Impinging jet calibration of excess shear sediment detachment parameters, *Trans. ASAE*, *40*(6), 1573–1580.

Stein, O. R., P. Y. Julien, and C. V. Alonso (1993), Mechanics of jet scour downstream of a headcut, *J. Hydraul. Res.*, *31*(6), 723–738.

Tucker, G. E., S. T. Lancaster, N. M. Gasparini, and R. L. Bras (2001), The channel-hillslope integrated landscape development (CHILD) model, in *Landscape Erosion and Evolution Modeling*, edited by R. S. Harmon and W. W. I. Doe, pp. 349–388, Springer, New York.

R. L. Bras and J. H. Flores-Cervantes, Department of Civil and Environmental Engineering, MIT, Room 48-212, Cambridge, MA 02139, USA. (homefc@mit.edu; rlbras@mit.edu)

E. Istanbulluoglu, Department of Geosciences, University of Nebraska at Lincoln, 200 Bessey Hall, Lincoln, NE 68588, USA. (erkan2@unl.edu)